remote sensing

Article

Impact of Speed and Differential Correction Base Type on Mobile Mapping System Accuracy

Luis Iglesias [1], Serafín López-Cuervo [2], Roberto Rodríguez-Solano [3] and Maria Castro [4,*]

[1] Departamento de Ingeniería Geológica y Minera, Universidad Politécnica de Madrid, 28003 Madrid, Spain; luis.iglesias@upm.es
[2] Departamento de Ingeniería Cartográfica, Geodésica y Fotogrametría, Universidad Politécnica de Madrid, 28031 Madrid, Spain; s.lopezc@upm.es
[3] Departamento de Ingeniería y Gestión Forestal y Ambiental, Universidad Politécnica de Madrid, 2804 Madrid, Spain; roberto.rodriguezsolano@upm.es
[4] Departamento de Ingeniería del Transporte, Territorio y Urbanismo, Universidad Politécnica de Madrid, 28040 Madrid, Spain
* Correspondence: maria.castro@upm.es

Highlights

What are the main findings?

- The study demonstrates that both operational conditions and GNSS correction strategies influence the positional accuracy of Mobile Mapping Systems (MMSs).
- Speed of data acquisition is identified as a key factor affecting overall mapping precision.

What are the implications of the main findings?

- The results provide practical guidance for improving the reliability of MMS-based surveys.
- Maintaining controlled operating conditions enhances the quality of spatial data used in road mapping and infrastructure applications.

Abstract

Mobile Mapping Systems (MMSs) have emerged as indispensable instruments for producing high-precision road maps in recent years. Despite incorporating modern devices, their efficacy may be influenced by operational variables such as vehicle speed or the type of GNSS (Global Navigation Satellite System) differential correction employed. This study assesses the impact of varying vehicle speeds and differential correction settings on the accuracy of point grids acquired with an MMS on a two-lane rural road. The experiment was performed across a 7 km distance, incorporating two speeds (40 and 60 km/h) and two travel directions. Three correction methodologies were examined: a proximate local base (MBS), a network station solution of the National Geographic Institute (NET), and virtual reference stations (VRSs). The methodology encompassed normality analysis, descriptive statistics, mean comparisons, one- and two-factor analysis of variance (ANOVA), and the computation of the root mean square error (RMSE) as a measure of accuracy. The findings indicate that horizontal discrepancies remain steady and unaffected by the correction technique; however, notable changes are seen in the vertical component, with the NET option proving to be the most effective. The acquisition rate is the primary determinant, exacerbating errors at 60 km/h. In conclusion, the dependability of MMS surveys is contingent upon the correction approach and operational conditions, and it is advisable to sustain moderate speeds to guarantee precise three-dimensional models.

check for updates

Academic Editor: Giuseppe Casula

Received: 5 November 2025
Revised: 11 December 2025
Accepted: 13 December 2025
Published: 18 December 2025

Citation: Iglesias, L.; López-Cuervo, S.; Rodríguez-Solano, R.; Castro, M. Impact of Speed and Differential Correction Base Type on Mobile Mapping System Accuracy. *Remote Sens.* **2025**, *17*, 4064. https://doi.org/10.3390/rs17244064

Copyright: © 2025 by the authors. Licensee MDPI, Basel, Switzerland. This article is an open access article distributed under the terms and conditions of the Creative Commons Attribution (CC BY) license (https://creativecommons.org/licenses/by/4.0/).

Keywords: Mobile Mapping System (MMS); road surveying; road mapping; geospatial accuracy

1. Introduction

The growing integration of technologies such as remote sensing, photogrammetry, and mobile mapping systems in geotechnical engineering and managing linear infrastructure, such as roads, highlights the value of having accurate and reliable three-dimensional models. Mobile Mapping Systems (MMSs) have become a key component of modern geospatial technologies, combining advanced sensor integration, efficient computational processing, and refined modelling techniques. Continuous advancements in hardware design, data fusion methodologies, and automation have strengthened MMS's analytical capability and operational efficiency, establishing them as versatile instruments for precise spatial data acquisition and comprehensive environmental modelling [1]. Tools such as Interferometric Synthetic Aperture Radar (PS-InSAR), which allows persistent dispersers to be identified in stable infrastructure, and Structure from Motion (SfM) photogrammetry workflows, capable of generating dense point clouds and high-resolution orthomosaics from Unmanned Aerial Vehicles (UAVs) or portable systems, have proven effective in characterizing deformations and landslides in seismic and post-disaster contexts [2].

In recent years, Mobile Mapping Systems (MMSs) have established themselves as key tools in generating high-precision road mapping. These systems, which integrate GNSS (Global Navigation Satellite System) sensors, inertial measurement units (IMUs), cameras, and laser scanners, enable the efficient and geo-referenced acquisition of spatial data from moving vehicles. This capability has significantly transformed traditional surveying methods and driven their adoption in producing next-generation road maps, such as high-definition maps (HD Maps) used in advanced mobility applications [3].

The development of laser scanning technology has transformed spatial data acquisition methods, establishing itself as a valuable tool in various applied areas. In the field of linear infrastructure, one of the most relevant applications is the use of Mobile Laser Scanners (MLSs) installed on moving vehicles, capable of generating high-resolution three-dimensional representations of the road environment. Although the process produces a high degree of measurement redundancy inherent to the principle of laser scanning, this surplus increases the density and continuity of point clouds, improving geometric accuracy and fidelity in the characterization of road elements and their adjacent areas.

One of the fundamental aspects of road mapping using MMS is positioning accuracy. The integration of GNSS/INS navigation has made it possible to achieve sub-decimetre accuracies under optimal conditions. However, in dense urban environments or in areas with dense tall vegetation, where GNSS signals may be degraded, specific strategies have been developed to mitigate these effects and improve the consistency of the collected data, such as the use of ground reference points [4,5] or a Zero velocity UPdaTe (ZUPT) module [6]. Other approaches have been proposed by automatically georeferencing MMS data through feature-based registration with aerial imagery, offering robust solutions for urban mapping scenarios [7]. These solutions, such as correcting deviations in redundant data, have proven to be effective in complying with the official cartographic standards required by national institutions [4]. Comparative analyses of professional and low-cost GNSS receivers, including smartphone-based sensors, demonstrate the potential of affordable devices for kinematic positioning, while highlighting that their performance is strongly influenced by environmental conditions [8].

Recent advances in GNSS theory have highlighted the need to refine both the functional and stochastic formulations of observation models, particularly in environments affected by multipath, diffraction, signal obstruction, and other sources of unmodelled error. In this regard, a recently proposed resilient RTK framework [9] incorporates these effects directly into the double-difference observation equations and their associated variance–covariance structures, enabling a more robust estimation process under degraded measurement conditions. This formulation integrates equality and inequality constraints to dynamically restrict the solution space according to physically admissible coordinate evolution, thereby improving ambiguity resolution rates and enhancing the statistical reliability of the resulting positions. Such developments underscore the importance of analyzing how different differential correction strategies influence MMS positional accuracy, especially in road environments where GNSS signal quality exhibits strong spatial and temporal variability.

On the other hand, the way these sensors are combined varies between manufacturers, and the quality of the data generated is highly dependent on the software that processes the information. Therefore, knowing the technical specifications of the sensors is not enough to estimate the system's accuracy. It is necessary to evaluate the MMS's actual performance by assessing the accuracy of the point clouds in the environment where it will be used [3]. The need to validate the real performance of an MMS has also been highlighted in previous studies, such as the SITEGI project, where sensor integration and georeferencing were assessed through the synchronization of GPS time, odometry, and IMU-based event tagging to ensure the geometric consistency of the acquired data [10].

Sensor calibration is another critical component in the reliability of the resulting geometric model. Various studies have proposed both manual and automated calibration methods, ranging from relative orientation techniques between cameras and GNSS/INS sensors [11,12] to fully automatic schemes based on the detection of geometric features in the environment, such as planes and lines present in urban facades or road structures [13–15]. Likewise, simplified approaches based exclusively on GNSS receivers have been developed, which allow extrinsic calibration to be resolved without requiring complex multi-sensor configurations [16]. Automated profile-based calibration strategies have been proposed without requiring specific targets or environmental features [17]. Other studies have explored the use of terrestrial laser scanners as an external reference for calibrating MMS, demonstrating their usefulness in improving the geometric accuracy of the systems [18]. These methodologies have significantly improved the spatial alignment between sensors and, consequently, the quality of the final mapping product. Likewise, simultaneous calibration schemes have been proposed on complex platforms that integrate multiple LiDAR sensors and cameras to optimize spatial consistency between all devices and ensure greater robustness in data capture.

MMS's ability to accurately identify and map road centrelines, road markings, and street furniture elements is particularly relevant for road mapping. Various MMSs have been designed specifically for this purpose, incorporating oriented cameras to stabilize the sampling geometry [6] and real-time processing algorithms that enable near-autonomous operations in road data collection [6,19]. Furthermore, integrating advanced processing techniques has expanded MMS applications toward infrastructure assessment, including LiDAR-based degradation modelling of road markings [20] and the real-time detection of peeling and delamination on infrastructure surfaces through combined 1D signal and 2D image processing methods [21].

Some authors have proposed using specialized facilities to systematically evaluate the accuracy of MMS used on roads. These facilities allow the validation of different systems under controlled conditions, identifying variations in performance associated with

sensor configurations or vehicle models [3]. In turn, evaluation methods have evolved from classical statistical analyses towards non-parametric approaches that provide a more faithful representation of errors in real scenarios [5].

Overall, advances in positioning, calibration, and accuracy assessment have consolidated the role of MMS as a robust and versatile tool for road mapping. Their ability to generate three-dimensional data with high spatial and temporal fidelity positions them as fundamental elements in developing smart infrastructures, advanced navigation systems, and urban planning.

Mobile Laser Scanning (MLS) systems have proven to be a reliable and cost-effective alternative to traditional airborne or UAV-based methods for mapping and inspection tasks, particularly in rural environments where aerial operations may be limited or unsafe [22]. These systems offer comparable or even superior geometric accuracy and spatial detail, enabling efficient data acquisition from ground-based platforms while maintaining high levels of positional precision. This demonstrates the strong potential of mobile mapping technologies as practical tools for producing accurate three-dimensional representations of linear infrastructure under diverse operational conditions.

In road mapping, positioning accuracy is a determining factor to guarantee the quality of the products derived from it, especially when seeking to generate reliable three-dimensional models for analysis and advanced applications, such as their use for generating scenarios for driving simulators. Although current MMSs integrate high-quality GNSS/INS solutions, their performance can be conditioned by operational factors, such as vehicle speed, and by the type of processing data acquired in the field, such as differential GNSS corrections. Global position correction in mobile mapping systems is typically performed using nearby GNSS reference stations to enhance positioning accuracy. This approach compensates for navigation errors caused by atmospheric effects, satellite ephemerides, or signal loss, and post-processing the onboard GNSS data with reference observations ensures accurate georeferencing of the acquired data [23]. In this context, it is essential to analyze how results vary when different correction configurations are used, including local bases, physical bases, or virtual reference stations (VRSs). This work aims to evaluate the influence of these variables on the accuracy of point grids generated from data acquired in the field by an MMS, on a two-lane rural road (the M-611 road, between Soto del Real and Miraflores, in the Community of Madrid, Spain).

The main objective of this study is to evaluate the combined effect of the acquisition speed and the type of differential correction on the positional accuracy of the point grids generated by an MMS in a real road environment. For this purpose, data obtained at speeds of 40 km/h and 60 km/h are analyzed using three correction strategies: a local base installed near the road, a network solution, and a VRS. The Spanish National Geographic Institute (IGN) provided the latter two. It also seeks to compare the performance of each configuration, identify the advantages and limitations associated with each method, and, finally, propose technical recommendations that will help to optimize both the data acquisition and processing processes in future road mapping projects using MMS technologies.

This study seeks to contribute to the continuous improvement of mobile mapping practices by proposing a structured evaluation of how acquisition parameters and correction strategies affect the positional accuracy of MMS-derived point clouds. The presented approach aims to enhance the reliability and consistency of spatial data generated in real road environments, offering practical guidelines to optimize field acquisition and subsequent processing stages. These advances are expected to strengthen the use of mobile mapping technologies in the precise modelling and monitoring of linear infrastructure.

2. Materials and Methods

The section under consideration corresponds to approximately 7 km of the M-611 road, which connects Soto del Real with Miraflores de la Sierra, in the Sierra de Guadarrama (Community of Madrid). It is a two-lane mountain road, with a winding layout characterized by sharp bends, changes in grades, and tiny hard shoulders, with ditches very close to the road. It has an Annual Average Daily Traffic (AADT) of over 5400 vehicles [24], with peak traffic on weekends and holidays. The environment is predominantly mountainous and forested, with masses of pine and holm oak trees, and is located within the area of influence of the Parque Nacional Sierra de Guadarrama. Figure 1 shows a picture of the roadway section and the sketches of the horizontal and vertical alignments.

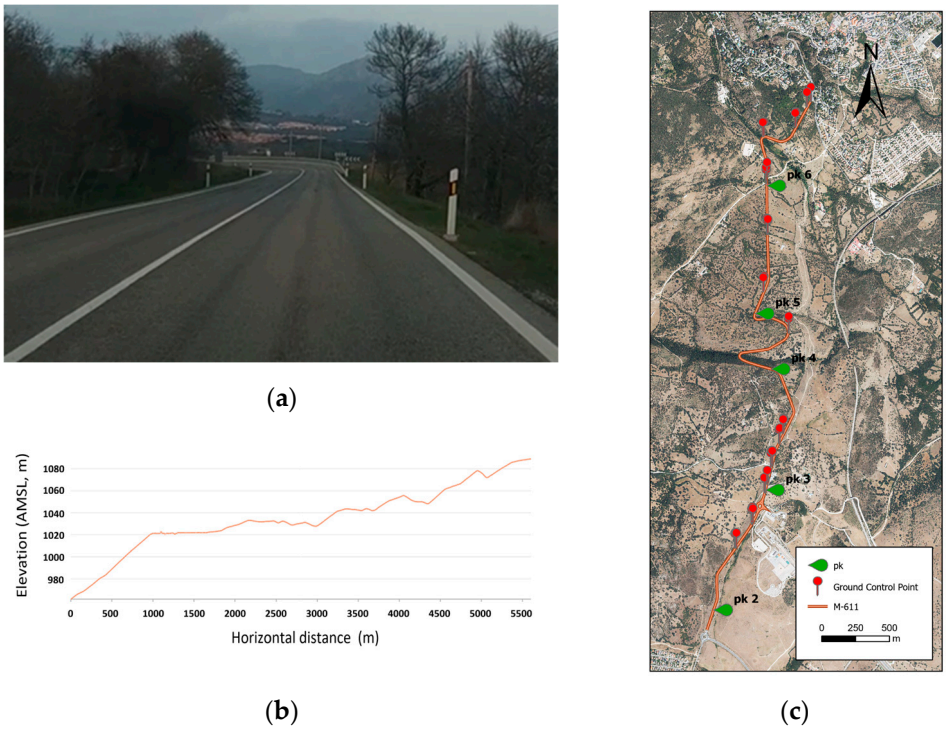


Figure 1. (**a**) Roadway section, (**b**) road vertical alignment, (**c**) road horizontal alignment. Base map for the road horizontal alignment derived from PNOA orthoimage (2023), provided by the Instituto Geográfico Nacional (IGN)/Centro Nacional de Información Geográfica (CNIG), under CC-BY 4.0 licence [25].

The capture system used (Figure 2) consisted of an MMS installed on a ground vehicle, equipped with high-precision sensors to acquire geometric and visual data simultaneously.

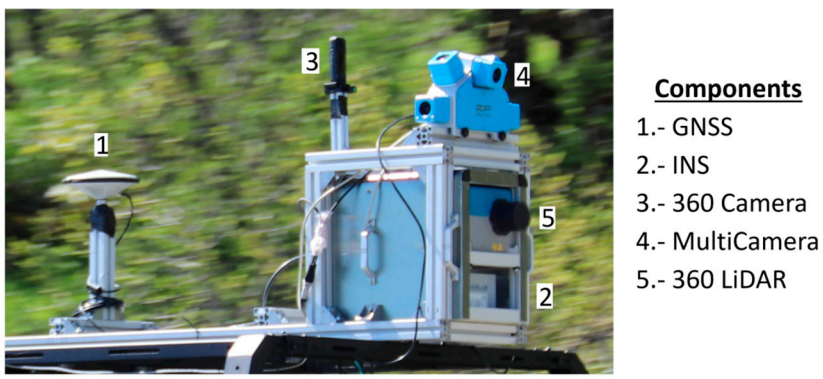


Figure 2. The MMS System installed in the vehicle and capturing the data.

The main component was the Z+F PROFILER® 9020 laser scanner (Zoller + Fröhlich GmbH, Wangen im Allgäu, Germany) [26], designed specifically for mobile mapping applications. This device provides a 360° field of view. It achieves a rotational capacity of up to 267 profiles per second (equivalent to 16,020 rpm), recording up to one million points per second. It has a maximum range of 182 m, with an accuracy of 0.2 mm, and incorporates optics intended for short-range measurements. In addition, its compact design, low power consumption, and short start-up times make it an efficient solution for data acquisition in road environments.

The system has a dual-frequency multi-constellation GNSS receiver (Navstar and GLONASS), operating at a sampling rate of 10 Hz. This equipment allowed the vehicle's trajectories to be recorded and subsequently refined using differential processing in PPK mode, as is customary in Mobile Mapping System (MMS) workflows. The accuracy of the GNSS solutions was increased by integrating them with data from the Inertial Navigation Unit (INS), which provides high-frequency measurements. The fusion of both sources of information made it possible to increase the temporal resolution of the trajectory from 10 Hz to approximately 300 Hz, thus obtaining a continuous and smoothed navigation solution that served as a reference for the correct georeferencing and integration of the LiDAR point clouds.

The iXBlue ATLANS-C [27] positioning and guidance unit combines a fibre optic inertial gyro system (FOG-INS) with a multi-constellation GNSS receiver compatible with GPS, GLONASS, SBAS, RTK, and TERRASTAR. According to the manufacturer's specifications, the system is capable of achieving angular accuracies of up to 0.02° in pitch, yaw and roll, and a horizontal accuracy on the order of 2 cm when operating in PPK mode. It can record data at frequencies up to 200 Hz with a latency of less than 3 ms, ensuring robust positioning even in urban environments with GNSS signal obstructions.

Imaging was performed using the Z+F MapCam® camera system (Zoller + Fröhlich GmbH, Wangen im Allgäu, Germany) [28]. This system is designed to integrate with the Z+F PROFILER® 9012, allowing simultaneous mapping of colour information on the captured measurement data. This system incorporates high-resolution sensors and a wide field of view, covering the entire measurement area. Its high capture speed makes it possible to obtain sharp, continuous images even at speeds of up to 90 km/h.

The data acquisition procedure started with route planning, defining the road section under study, lighting conditions, and travel speed. The car, equipped with the MMS, travelled the route at a constant speed, which ensured the necessary point density and minimized possible errors due to vibrations or blurring of the images.

During the field campaign, the Z+F PROFILER® 9020 laser scanner (Zoller + Fröhlich GmbH, Wangen im Allgäu, Germany) generated real-time cross-sectional profiles of the environment, while the MapCam cameras recorded synchronized images. In parallel, the ATLANS-C unit provided precise georeferencing of each captured point. All information was stored in the on-board control unit, integrating geometric, positional, and visual data.

The data obtained were subsequently preprocessed by the company responsible, Urquizo [29], for the acquisition, eliminating noise and redundancies, which allowed a purified point cloud to be generated. In particular, the data corresponding to the M-611 road were collected through two complete journeys between the roundabout at the exit of Soto del Real and the town of Miraflores de la Sierra, both in the outward and return directions. These journeys were made at two different speeds: 40 km/h for the first and 60 km/h for the second. The study was designed to keep speeds as constant as possible, avoiding acceleration and deceleration phases that could introduce additional errors. The selected speeds, 40 km/h and 60 km/h, were chosen to assess whether vehicle speed—being directly related to measurement noise and variations in profile

determination—affects the results. Given the characteristics of the road, higher speeds (e.g., 90 km/h) were neither safe nor feasible due to its winding layout and traffic conditions.

During the outbound journey, the right lane was recorded with the LiDAR system in a zenith position (perpendicular to the road surface). In contrast, the left lane was captured from an oblique angle. As shown in Figure 3, the perpendicular acquisitions are represented in blue, while the oblique acquisitions are depicted in red. On the return journey, the arrangement was reversed: the right lane (which corresponded to the left lane on the outward journey) was recorded from a zenith view, and the left lane was captured this time from an oblique angle. In this study, the lane along which the capture vehicle travels will be called Outbound, while the opposite lane will be called Inbound. This strategy allowed for redundant and complementary coverage of both lanes, ensuring a comprehensive survey of the study section. Consequently, each road lane was captured in four different situations, combining two traffic speeds and two capture angles (zenith and oblique). Figure 3 illustrates the data acquisition strategy described in the text, and Table 1 summarizes all field data collection situations.

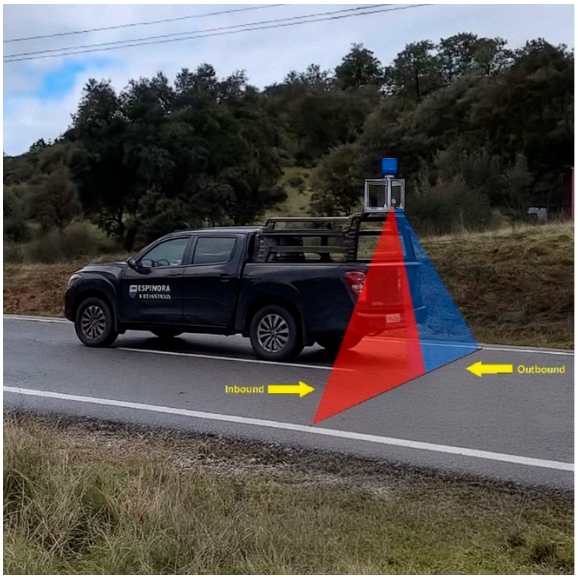


Figure 3. Schematic representation of the road survey configuration.

Table 1. Summary of survey conditions for data acquisition along the M-611 road. The travel from Soto del Real to Miraflores de la Sierra is the outbound direction, and the travel from Miraflores de la Sierra to Soto del Real is the inbound direction.

Direction of Travel	Speed (km/h)	Lane	Capture Angle
Outbound	40	Right	Vertical
		Left	Oblique
	60	Right	Vertical
		Left	Oblique
Inbound	40	Right	Vertical
		Left	Oblique
	60	Right	Vertical
		Left	Oblique

The survey was carried out in both travel directions along the road—referred to as *outbound* and *inbound*—and each direction was recorded at two speeds (40 km/h and 60 km/h). These terms describe the vehicle's direction of movement, while the lane

designation corresponds to the lane being captured in each pass. The combination of these acquisition conditions, together with the different processing strategies, defines the set of survey cases summarized in Table 1.

The system's data underwent a pre-processing process to ensure accurate georeferencing. For this purpose, the company responsible for the acquisition applied three georeferencing methods.

The first method used consisted of applying a local differential correction, obtained from data recorded by a GNSS station temporarily installed near the road on the same day as the data acquisition. This configuration enabled the generation of highly accurate corrections synchronized with the vehicle path, minimizing potential errors associated with temporal or spatial variations between the base and the mobile receiver. This approach is referred to as the Mobile Base Station configuration and, for simplicity, it will be designated hereafter as MBS.

The second method was based on using an RTK (Real-Time Kinematic) system with VRS provided by the IGN (Figure 4). This approach makes it possible to generate a virtual reference station located in the vicinity of the mobile receiver from data obtained from a network of GNSS stations distributed over the territory. Thanks to this, precise corrections are obtained in real time, which significantly improves positioning accuracy. In this work, this procedure will be referred to as VRS.

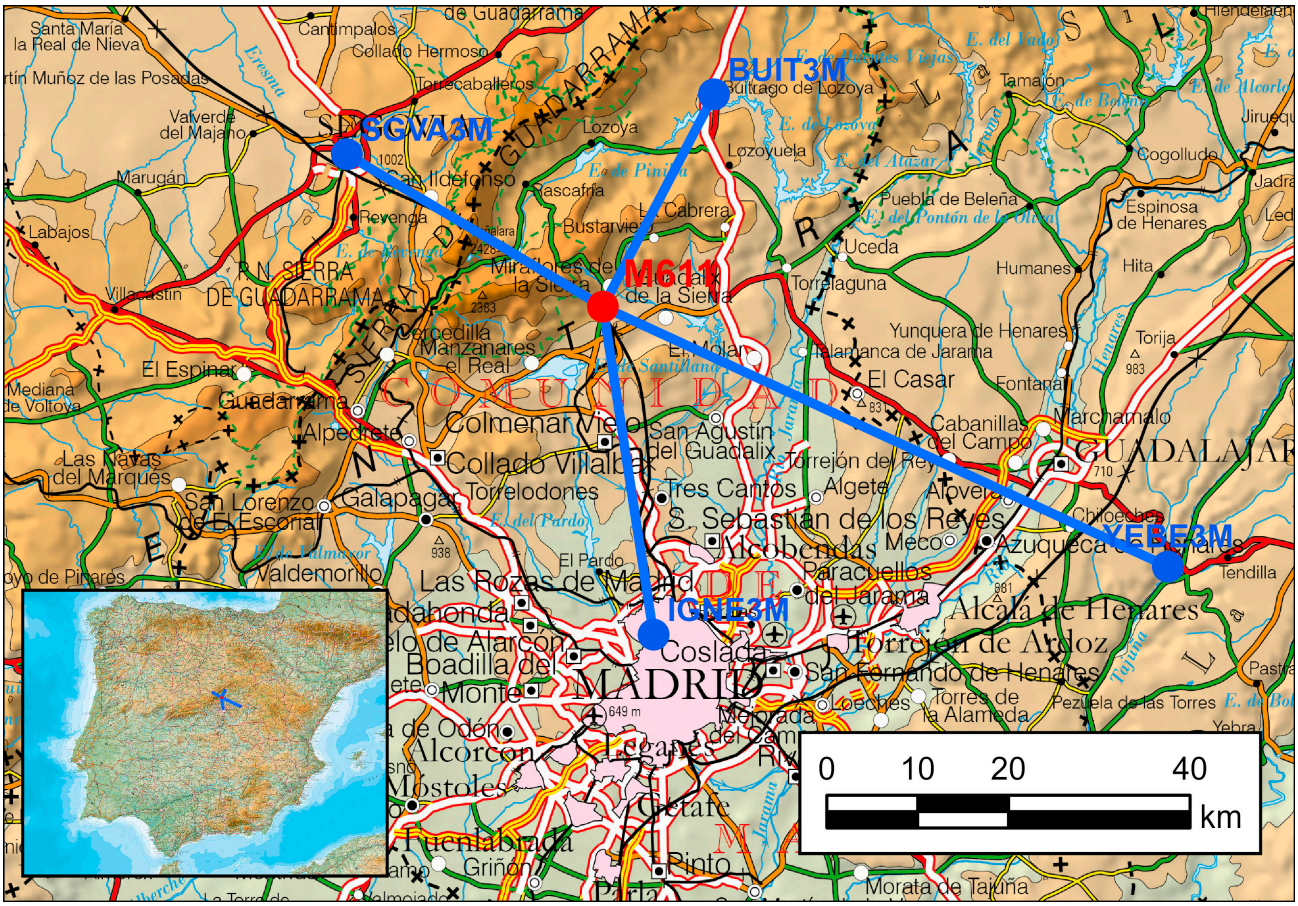


Figure 4. Spanish Geographic Institute base stations used in the VRS Solution. Base map from Map of the Iberian Peninsula and Balearic Islands, scale 1:1,250,000 (2022), provided by the Instituto Geográfico Nacional (IGN)/Centro Nacional de Información Geográfica (CNIG), under CC-BY 4.0 licence [25].

The third and last method was based on differential georeferencing in RTK mode using data from the permanent station of the GNSS network managed by the IGN. By providing

continuous and high-quality data, this station allowed an accurate differential correction to be made while processing the data acquired by the mobile system. This approach will be referred to hereafter as NET for ease of identification throughout this work.

All MMS acquisitions were performed during the same survey sessions, using the same equipment, identical hardware configurations, and common GNSS/INS parameters, ensuring identical satellite geometry, atmospheric conditions, and constellation availability across all cases. Under these controlled conditions, the only methodological difference among solutions is the source of differential corrections. The three strategies analyzed—MBS, NET and VRS—represent the complete set of differential GNSS correction modes operationally available for the MMS and the Spanish reference network, thus covering the full spectrum of relevant configurations for road-mapping applications.

Figure 4 summarizes the mean baseline distances associated with each correction strategy, given that baseline length is a key factor influencing the quality of differential GNSS processing. For the VRS configuration, the IGN network stations are located approximately 40 km from the study area. In the NET approach, the nearest permanent station solution lies at about 7 km for the acquisition of control points and approximately 3 km for the LiDAR surface-processing section. In contrast, the MBS configuration employed a locally installed base station positioned in the immediate vicinity of the survey area, resulting in significantly shorter baselines.

In addition to the general description of the three correction strategies, it is important to highlight their operational differences. The NET configuration applies a post-processed kinematic (PPK) workflow based on simultaneous observations from a distributed network of permanent GNSS stations, enabling trajectory reconstruction with the support of spatially redundant reference data. In contrast, the MBS approach also relies on PPK but uses a single local base station positioned in the immediate vicinity of the survey area, eliminating network redundancy but minimizing baseline length. Finally, the VRS strategy derives its corrections from the same GNSS infrastructure used by NET, although the network observations are processed to generate a virtual reference station located near the rover. This allows centimetric-level corrections to be delivered in real time, representing the key distinction from PPK-based solutions, which require deferred processing. Virtual Reference Station (VRS) services are widely used in Network RTK positioning and are designed to reduce the effective baseline between the rover and reference station while incorporating atmospheric modelling from surrounding CORS stations. This approach provides centimetric accuracy in typical operational conditions and represents one of the most established differential correction methodologies used in modern GNSS applications [30].

Once the GNSS trajectories have been obtained—whether through post-processed or real-time differential strategies—the MMS integrates measurements from the onboard INS sensors to refine the trajectory, stabilize the navigation solution, and enable accurate alignment of the resulting LiDAR point clouds. This GNSS/INS integration workflow is identical across all configurations, regardless of vehicle speed or direction of travel. Consequently, differences in the final point cloud accuracy arise exclusively from the manner in which the initial GNSS trajectory is determined, from the degree to which the INS contributes to its refinement, and from the subsequent polar-based LiDAR processing inherent to MMS post-processing.

Two independent studies were designed to evaluate the influence of differential correction strategies on the georeferencing accuracy of point clouds. In the first study, the analysis focused on comparing the three correction methods (MBS, VRS, and NET) using the outbound trajectory at a constant speed of 40 km/h (MBS40O, VMS40O, and S40O). In the second study, the V60 configuration was selected following the proposal of the company in charge of the field data acquisition. This approach aimed to evaluate the performance of

their equipment and the applied differential correction method while relying exclusively on autonomous receivers, independent of base stations or reference networks managed by other organizations. For this configuration, disaggregated datasets were analyzed for both acquisition speeds (40 and 60 km/h) and both traffic directions (outbound and inbound), resulting in the cases MBS40O, MBS40I, MBS60O, and MBS60I. In contrast, the analyses involving VRS and NET strategies were restricted to the outbound trajectory at 40 km/h to maintain a consistent and comparable framework across methods. For each configuration, the company in charge of data acquisition generated the corresponding georeferenced point clouds, which were subsequently used for the identification, organization, and detailed statistical analysis of each evaluated scenario. Table 2 summarizes the cases considered and the coding scheme applied in the subsequent statistical analysis.

Table 2. Coding of Survey Cases by Georeferencing Method, Speed, and Direction of Travel.

Case	Georeferencing Method	Speed (km/h)	Direction
MBS40O	MBS	40	Outbound
MBS40I	MBS	40	Inbound
MBS60O	MBS	60	Outbound
MBS60I	MBS	60	Inbound
VRS40O	VRS	40	Outbound
NET40O	NET	40	Outbound

For clarity, it should be noted that the NET solution was obtained using post-processed corrections from the nearest permanent IGN station; the VRS solution relied on the interpolated corrections generated by the IGN network, creating a virtual base in the same position as the third method; and the MBS configuration used a local temporary base station installed in the immediate vicinity of the survey area. These three strategies represent distinct operational scenarios commonly considered in MMS applications and were applied consistently to all datasets.

Control points distributed along the analyzed stretch of road were acquired to evaluate the positional accuracy of the models generated using LiDAR technology. For this purpose, the coordinates were determined with high precision (using RKT GNSS equipment) of points located on the road markings, specifically on both sides of the carriageway. Both the base station and the mobile receiver used to obtain the control point data were Zenith Z40 models manufactured by GEOMAX (Widnau, Suiza, Switzerland), with technical specifications equivalent to those described above; these devices are presented in Figure 5. The points selected corresponded to the outer vertices of the boundary lines of the pavement markings to guarantee their unequivocal identification when locating them on the point clouds. Thirty-eight control points were identified and recorded, evenly distributed along the entire study section, providing a reliable basis for the geometric accuracy analysis. The spatial distribution of these points is presented in Figure 1, superimposed on the road horizontal alignment.

The coordinates of the control points were determined using the RTK and VRS methods, with 20 measurements per point and an interval of 0.5 s between them. The equipment was a GeoMax Zenith40 receiver (GeoMax AG, Widnau, Suiza, Switzerland) [31], a rugged and high-performance multi-constellation GNSS device, equipped with a NovAtel OEM7 555-channel engine, providing compatibility with GPS, GLONASS, BeiDou, Galileo, QZSS, and NavIC satellite systems. The GNSS positioning results demonstrate high geolocation accuracy, with a mean horizontal root mean square (HRMS) error of 0.015 m and a vertical root mean square (VRMS) error of 0.025 m. These values reflect the positional accuracy in the horizontal and vertical planes, respectively. In addition, the average normalized

(NRMS) and ellipsoidal (ERMS) errors were 0.011 m and 0.010 m, respectively, indicating good consistency in observations and position with respect to the geodetic model. The average number of satellites used was 15.6, ensuring sufficient coverage for accurate and reliable localisation. Table 3 shows the quality parameters of the GNSS measurements.



Figure 5. Base and Rover GEOMAX Zenith 40 [31].

Table 3. Statistical Summary of GNSS Measurement Accuracy.

Parameter	Mean (m)	Minimum (m)	Maximum (m)
HRMS—Horizontal Root Mean Square	0.015	0.011	0.034
VRMS—Vertical Root Mean Square	0.025	0.018	0.077
NRMS—Normalized Root Mean Square	0.011	0.008	0.025
ERMS—Ellipsoidal Root Mean Square	0.010	0.006	0.023

A manual identification process was carried out in each of the point clouds to locate those points closest to the control points previously surveyed in the field. This identification was carried out taking as a reference the precise location of the control points and the chromatic values assigned to the points in the cloud by the capture system, which are generated from the photographic images recorded during the acquisition process. For each point identified, the evaluation variable was calculated, defined as the difference between the coordinates of the control point and the coordinates of the corresponding point in the cloud. The parameters were obtained from these coordinates: the discrepancy in the X component, the discrepancy in the Y component, and the discrepancy in the Z component. These values formed the basis for the analysis and comparison of the accuracy associated with each of the cases evaluated in the study.

Since the measurements were obtained using GNSS receivers, it was considered appropriate to integrate the discrepancies in the X and Y components into a NET planimetric indicator. In this study, the nomenclature Horizontal discrepancy refers to this integrated component, which represents the differences between the GNSS-measured values and those derived from the mesh for the X and Y axes of the coordinate system. Conversely, the Z component is treated independently and referred to as Vertical discrepancy, denoting the differences in elevation relative to the same coordinate system. This decision is based on the anisotropic behaviour characteristic of this type of data, where horizontal accuracy is usually higher and more stable than vertical accuracy, as evidenced by the values

obtained (mean HRMS of 0.015 m versus a mean VRMS of 0.025 m, with maxima of 0.034 m and 0.077 m, respectively, as shown in Table 3). Aggregating X and Y allows for a synthetic description of horizontal error without losing relevant information, while isolating the vertical component avoids masking its higher variability and ensures a more accurate analysis.

From a methodological standpoint, the advanced observation models and statistical formulations presented in recent GNSS research [9] provide a rigorous theoretical basis for interpreting the behaviour of double-difference measurements under heterogeneous signal conditions. These formulations explicitly describe how unmodelled errors—such as multipath, diffraction, non-line-of-sight reception, and residual atmospheric effects—propagate through both the functional model and the variance–covariance structure, generating anisotropic error distributions and differential sensitivity between horizontal and vertical components. Although the present study does not implement constraint-based RTK filtering, the principles derived from these refined observation and stochastic models justify the separate evaluation of planimetric and vertical discrepancies, as well as the comparative assessment of multiple differential correction strategies (MBS, NET, VRS). This connection is particularly relevant because vertical accuracy is more susceptible to covariance deformation and unmodelled residuals, behaviour consistent with the statistical characteristics described in these enhanced GNSS formulations.

The methodology adopted for the two proposed analyses is structured in several successive stages. First, the normality of the variables will be assessed to verify the statistical assumptions required for subsequent procedures. Then, a descriptive statistical analysis will be performed, including central tendency and dispersion measures, complemented by graphical representations to facilitate comparison between strategies and experimental conditions. Afterwards, mean comparison tests will be applied to identify potential significant differences between groups, and an analysis of variance (ANOVA) will be conducted to contrast discrepancies among multiple configurations simultaneously. This methodological sequence will be implemented independently for the two studies, ensuring a systematic and consistent approach to evaluating the different differential correction strategies and acquisition conditions.

Figure 6 presents an overview of the materials, methods, and analytical procedures employed in this study. It summarizes the equipment used, the data acquisition process, the georeferencing strategies implemented, and the subsequent evaluation of differential correction methods and driving conditions.

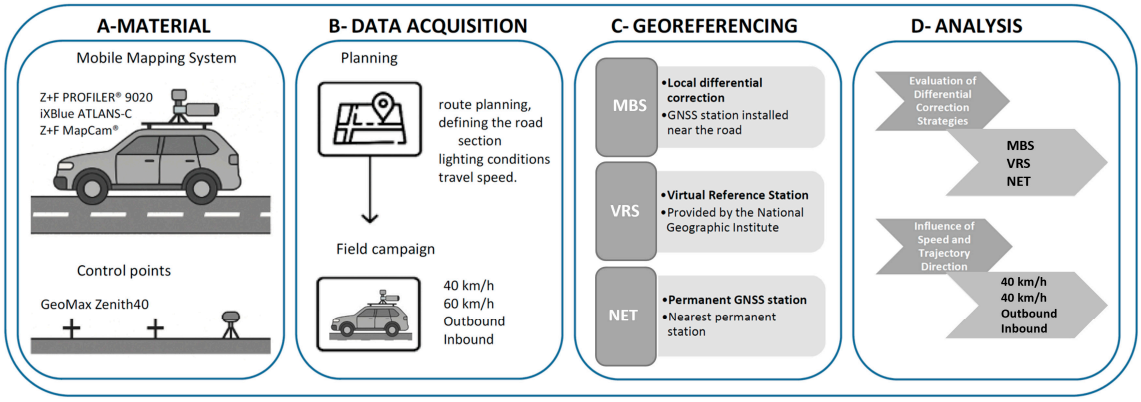


Figure 6. Schematic of the Study Approach.

3. Results

First, the evaluation of differential correction strategies is presented, followed by the influence of speed and trajectory direction.

3.1. Evaluation of Differential Correction Strategies

The statistical characterization of the discrepancies and the comparative performance of the correction strategies are presented. The analysis emphasizes both the central tendency and dispersion of the data, as well as the existence of potential biases, to establish the relative accuracy of each method.

The Shapiro–Wilk normality test was applied to the Horizontal and Vertical discrepancy under the three GNSS Differential Correction Strategies (NET, VRS, MBS). The results indicate that, in general, both variables follow a normal distribution ($p > 0.05$), with the only exception being the Horizontal discrepancy under the NET strategy, where $p = 0.010$. However, considering the overall consistency of the results and the robustness of parametric tests to slight deviations from normality, both variables will be treated as normally distributed in the subsequent analyses. Table 4 presents the results of the normality test. Table 5 shows the descriptive statistics for both horizontal and vertical discrepancies by differential correction strategy considered.

Table 4. Shapiro–Wilk Test for Normality of Discrepancies by Correction Strategy.

Correction Strategy	Variable	*p*-Value	Normality ($\alpha = 0.05$)
NET	Horizontal discrepancy	0.010	H0 (Normality) is rejected
	Vertical discrepancy	0.764	H0 (Normality) is accepted
VRS	Horizontal discrepancy	0.095	H0 (Normality) is accepted
	Vertical discrepancy	0.289	H0 (Normality) is accepted
MBS	Horizontal discrepancy	0.564	H0 (Normality) is accepted
	Vertical discrepancy	0.988	H0 (Normality) is accepted

Table 5. Descriptive Statistics of Horizontal and Vertical discrepancies by Differential Correction Strategy.

Descriptive Statistic		Differential Correction Strategy		
		MBS	VRS	NET
Horizontal discrepancy (m)	Mean	0.067	0.067	0.061
	Median	0.064	0.069	0.059
	Mode	0.012	0.012	0.007
	Standard deviation	0.031	0.031	0.028
Vertical discrepancy (m)	Mean	0.000	0.015	−0.021
	Median	0.000	0.020	−0.020
	Mode	−0.009	0.016	−0.020
	Standard deviation	0.021	0.038	0.046

The paired *t*-test analysis of horizontal discrepancy did not reveal statistically significant differences among the three evaluated methods (MBS, VRS, and NET). The comparisons between MBS and VRS ($p = 0.944$), MBS and NET ($p = 0.264$), and VRS and NET ($p = 0.131$) all indicated non-significant results, with mean Horizontal discrepancies ranging consistently between 0.06 and 0.07. These findings suggest that the three methods perform comparably in terms of planimetric accuracy, and no method demonstrates a clear advantage over the others. Results are displayed in Table 6.

Table 7 presents the results of the paired *t*-test analyses performed on the Vertical discrepancy values obtained with the three methods (MBS, VRS, and NET). The comparisons revealed significant differences among the methods across the vertical axis. VRS yielded the highest discrepancies, NET showed the lowest, and MBS remained close to zero. These outcomes emphasize the influence of the measurement method on vertical error estimation, highlighting that the three approaches differ systematically when evaluated along the Z dimension.

Table 6. Paired *t*-test results for Horizontal discrepancies across Differential Correction Strategy.

Comparison	Mean 1 (m)	Mean 2 (m)	Mean Difference (m)	Pearson r	t (37 df)	*p* (Two-Tailed)	Result
MBS vs. VRS	0.0668	0.0673	−0.0005	0.155	−0.07	0.944	Not significant
MBS vs. NET	0.0668	0.0613	0.0055	0.483	1.13	0.264	Not significant
VRS vs. NET	0.0673	0.0613	0.0060	0.671	1.54	0.131	Not significant

Table 7. Paired *t*-test results for vertical-axis discrepancies across Differential Correction Strategy.

Comparison	Mean 1 (m)	Mean 2 (m)	Mean Difference (m)	Pearson r	t (37 df)	*p* (Two-Tailed)	Result
MBS vs. VRS	0.00034	0.01545	−0.0151	0.684	−3.31	0.0021	Signif. difference
MBS vs. NET	0.00034	−0.02068	0.0210	0.636	3.58	0.0010	Signif. difference
VRS vs. NET	0.01545	−0.02068	0.0361	0.567	5.63	2.01×10^{-6}	Signif. difference

The paired *t*-test provides valuable information on differences between specific pairs of correction strategies, but does not capture the overall effect of the three methods when considered simultaneously. ANOVA offers a more comprehensive statistical framework, enabling the joint comparison of means across multiple groups under a NET global hypothesis test. This approach reduces the inflation of type I error that arises from conducting multiple pairwise tests independently and provides a more robust basis for inference.

In differential correction strategies, ANOVA is appropriate for Horizontal and Vertical discrepancies across the three methods (NET, VRS, and MBS). By testing for overall differences among groups, ANOVA determines whether the correction strategy has a statistically significant effect on the observed variables. When significant effects are identified, post hoc comparisons can then be employed to specify which methods differ.

The one-way ANOVA analyses were conducted to evaluate whether the choice of GNSS differential correction strategy (MBS, VRS, NET) significantly affected Horizontal and Vertical discrepancy. The results of these analyses are presented in Table 8.

Table 8. Summary of one-way ANOVA results for discrepancies across differential correction strategies.

Variable	Source of Variation	Df	Sum Sq (m^2)	Mean Sq (m^2)	F Value	*p*-Value	Signif.
Horizontal Discrepancy	Factor (Strategy)	2	0.00084	0.00042	0.472	0.6250	
	Error	111	0.09901	0.00089			
	Total	113	0.09985				
Vertical Discrepancy	Factor (Strategy)	2	0.02503	0.01251	9.389	0.0002	***
	Error	111	0.14794	0.00133			
	Total	113	0.17297				

Note: The significance codes indicate the level of statistical significance associated with the *p*-values as follows: *** for $p < 0.001$, ** for $p < 0.01$, * for $p < 0.05$, • for $p < 0.1$, and a blank space for $p \geq 0.1$, indicating no statistical significance.

The one-factor ANOVA revealed clear differences between horizontal and vertical discrepancies depending on the differential correction strategy applied. For the horizontal discrepancy, no statistically significant differences were found between the evaluated strategies ($F = 0.472,\ p = 0.625$). This result indicates that the type of correction employed did not have a meaningful impact on the horizontal accuracy of the collected data.

In contrast, for the vertical discrepancy, highly significant differences were observed ($F = 9.389,\ p < 0.001$), showing that the differential correction strategy has a significant influence on the vertical accuracy of the observations. These results suggest that, while

horizontal accuracy remains stable regardless of the approach used, vertical accuracy is more sensitive to the conditions or characteristics of the differential correction applied.

Since the ANOVA for the vertical discrepancy showed statistically significant differences between the differential correction strategies, Tukey's HSD (Honestly Significant Difference) test was applied. This post hoc analysis is particularly useful for identifying which pairs of strategies have significant differences in their means, thus allowing a controlled comparison that maintains the overall significance level and avoids the increase in Type I error associated with multiple contrasts.

The application of Tukey's test provides adjusted significance values and confidence intervals for each comparison, facilitating the interpretation of the results and the identification of statistically homogeneous groups. This approach is fundamental to solidly supporting the study's conclusions, as it allows objective discrimination of which differential correction strategies perform more accurately in terms of vertical discrepancy.

Table 9 presents the results of the pairwise comparisons performed using the Tukey HSD test for the vertical discrepancy variable. The data show that there is a statistically significant difference between the VRS and NET groups ($p < 0.001$), with a mean difference of 0.036 (95% CI 0.016–0.056), indicating that the VRS group has higher vertical discrepancy values. Similarly, a significant difference was observed between the MBS km/h and NET groups ($p = 0.036$), with a mean difference of 0.021 (95% CI 0.001–0.041). However, the comparison between MBS km/h and VRS showed no significant difference ($p = 0.173$), with a negative mean difference of −0.015 (95% CI −0.035–0.005). Taken together, these results suggest that both VRS and MBS km/h generate larger vertical discrepancies compared to NET, although there is no evidence of relevant differences between VRS and MBS km/h.

Table 9. Pairwise comparisons using Tukey's HSD for vertical discrepancy.

Variable	Comparison	Means Difference (m)	Lower Limit (m)	Upper Limit (m)	*p* Adjusted	Significance
Vertical Discrepancy	VRS—NET	0.036	0.016	0.056	0.000	Yes
	MBS—NET	0.021	0.001	0.041	0.036	Yes
	MBS—VRS	−0.015	−0.035	0.005	0.173	No

Based on the results presented in Table 9, Table 10 summarizes the analysis of the vertical discrepancy between the groups using ANOVA and Tukey's HSD post hoc tests. The results show statistically significant differences ($p < 0.001$) between the groups evaluated. The VRS group showed the highest values of vertical discrepancy, while the NET group showed the lowest values. On the other hand, the MBS group showed an intermediate behaviour, with no significant differences from the other two groups. In Table 10, the letters (a, ab, b) indicate the Tukey HSD grouping, where shared letters denote no significant difference and different letters indicate statistically distinct groups.

Table 10. Comparison between groups for vertical discrepancy using ANOVA and Tukey HSD post hoc testing.

Group	Assigned Letter
NET	a
MBS	ab
VRS	b

Note: Groups with different letters showed statistically significant differences ($p < 0.001$).

Figure 7 illustrates the distribution of horizontal and vertical discrepancies obtained for each differential correction strategy (NET, VRS and MBS) using box plots. In accordance

with the ANOVA results presented in Table 8, it is observed that, for the horizontal discrepancy, the distributions are similar between strategies, with no statistically significant differences. In contrast, the diagrams corresponding to the vertical discrepancy show notable variations between groups, with higher values for the VRS strategy, intermediate for MBS, and lower for NET, which coincides with the results of the multiple comparisons described in Tables 9 and 10.

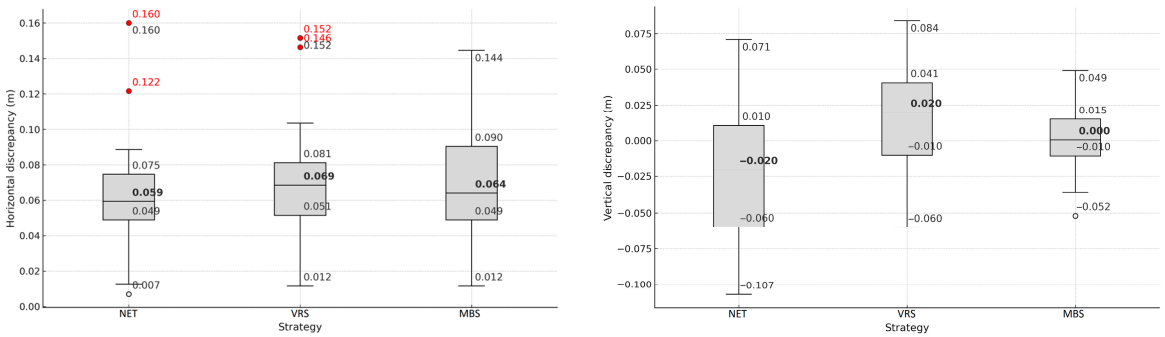


Figure 7. Distribution of the horizontal and vertical discrepancies obtained for each differential correction strategy (NET, VRS, and MBS) represented by boxplots. The red dots represent outliers. The bold values denote the statistical median.

The Root Mean Square Error (RMSE) was employed as an integrated indicator of positional accuracy to evaluate the relative performance of the correction strategies. A global RMSE was calculated by combining the Horizontal and Vertical discrepancies into a NET metric to obtain an integrated indicator of positional accuracy. This approach allows for the synthesizing of the different error components into one value, facilitating the comparative evaluation of the influence of the factors considered and their interactions. The RMSE global was computed according to Equation (1).

$$RMSE_{global} = \sqrt{\frac{\left(RMSE^2_{Horizontal\ discrepancy} + RMSE^2_{Vertical\ discrepancy}\right)}{4}} \quad (1)$$

Unlike the analysis of individual discrepancies, which examines errors separately for the horizontal and vertical discrepancies, RMSE provides a synthetic measure that simultaneously accounts for deviations in both components. This approach allows for a more comprehensive assessment of overall accuracy, as it penalizes larger deviations and highlights systematic differences among strategies. By summarizing error magnitudes into a NET metric, RMSE facilitates a direct and objective comparison of correction strategies, enabling the identification of the method that yields the closest agreement with the control points. The RMSE results for the analyzed values are presented in Table 11.

Table 11. RMSE values for the strategies considered.

Strategy	Horizontal Discrepancy (m)	Vertical Discrepancy (m)	RMSE (Z + Horizontal) (m)
MBS	0.0668	0.0003	0.0472
VRS	0.0673	0.0154	0.0488
NET	0.0613	−0.0207	0.0457

Table 11 summarizes the RMSE values obtained when considering both horizontal discrepancies and vertical (Z) errors. The results indicate that the NET strategy provides the lowest RMSE (0.0457), reflecting the best overall agreement with the control points. MBS shows an intermediate performance (0.0472), with horizontal discrepancies similar to

VRS but lower Z errors. In contrast, despite comparable horizontal accuracy, VRS yields the highest RMSE (0.0488), mainly due to larger deviations along the vertical axis. These findings suggest that NET offers the most balanced performance when both horizontal and vertical accuracy are considered simultaneously, while MBS performs adequately, but VRS appears more sensitive to vertical error.

3.2. Influence of Speed and Trajectory Direction

To evaluate the influence of the speed of displacement and the direction of the trajectory on the accuracy of the data obtained, a structured statistical methodology will be followed, starting with the verification of the normality of the variables, to determine the suitability of the parametric methods to be used. Subsequently, paired means comparison tests will be applied to identify significant differences between specific speed and trajectory conditions. An ANOVA will then be carried out globally to examine the effect of these factors and their possible interactions on the horizontal discrepancy. Finally, the RMSE will be calculated to quantify the magnitude of the error in a comprehensive manner and to facilitate comparison between different test scenarios.

The results of the Shapiro–Wilk test (Table 12) indicate that, in general, the distributions of the horizontal and Vertical discrepancies can be considered normal across most combinations of speed and lane. At 40 km/h, both discrepancies consistently met the normality assumption for inbound and outbound trajectories. Similarly, at 60 km/h, most cases accepted the null hypothesis of normality, except for the horizontal discrepancy in the inbound trajectory, where the *p*-value (0.045) was below the significance threshold ($\alpha = 0.05$). This suggests that while the data largely conform to a normal distribution, specific conditions—namely, higher speed and inbound direction—may introduce deviations that affect the distribution of horizontal discrepancies.

Table 12. Shapiro–Wilk Test for Normality of Discrepancies by speed and lane.

Speed (km/h)	Lane	Variable	*p*-Value	Normality ($\alpha = 0.05$)
40	Outbound	Horizontal discrepancy	0.564	H0 (Normality) is accepted
		Vertical discrepancy	0.988	H0 (Normality) is accepted
40	Inbound	Horizontal discrepancy	0.870	H0 (Normality) is accepted
		Vertical discrepancy	0.979	H0 (Normality) is accepted
60	Outbound	Horizontal discrepancy	0.073	H0 (Normality) is accepted
		Vertical discrepancy	0.751	H0 (Normality) is accepted
60	Inbound	Horizontal discrepancy	0.045	H0 (Normality) is rejected
		Vertical discrepancy	0.508	H0 (Normality) is accepted

Table 13 provides a concise summary of the results related to coordinate discrepancies, categorized by speed and trajectory direction.

A paired-samples mean comparison test was applied to determine whether there were statistically significant differences in the discrepancies as a function of vehicle speed during the capture of the meshes and the lane of traffic recorded. The results are presented in Table 14 for the speed analysis and Table 15 for the lane analysis.

Table 13. Descriptive statistics of coordinate discrepancies by speed and trajectory direction.

Descriptive Statistic		Speed (km/h)		Lane	
		40	60	Outbound	Inbound
Horizontal discrepancy (m)	Mean	0.067	0.092	0.076	0.084
	Median	0.065	0.082	0.069	0.077
	Mode	0.007	0.061	0.061	0.007
	Std. dev.	0.032	0.042	0.036	0.043
Vertical discrepancy (m)	Mean	0.000	−0.006	−0.005	−0.001
	Median	0.000	−0.005	−0.004	−0.001
	Mode	−0.011	−0.001	−0.009	−0.002
	Std. dev.	0.021	0.021	0.022	0.021

Table 14. Paired *t*-test results for discrepancies across speed.

Comparison	Mean 1 (m)	Mean 2 (m)	Mean Difference (m)	Pearson r	t (37 df)	*p* (Two-Tailed)	Result
Horizontal discrepancy (40 km/h vs. 60 km/h)	0.067	0.092	0.025	0.374	−5.02	3.36×10^{-6}	Significant difference
Vertical discrepancy (40 km/h vs. 60 km/h)	0.0003	−0.0063	−0.0066	0.873	5.38	8.1×10^{-7}	Significant difference

Table 15. Paired *t*-test results for discrepancies across trajectory direction.

Comparison	Mean 1 (m)	Mean 2 (m)	Mean Difference (m)	Pearson r	t (37 df)	*p* (Two-Tailed)	Result
Horizontal discrepancy (Outbound vs. Inbound)	0.076	0.084	0.0080	0.768	−2.62	0.0107	Significant difference
Vertical discrepancy (Outbound vs. Inbound)	−0.0053	−0.0008	0.0045	0.92	−4.59	1.73×10^{-5}	Significant difference

The paired samples *t*-test results (Tables 14 and 15) reveal statistically significant effects of both vehicle speed and traffic lane on the discrepancies analyzed. Regarding speed, significant differences were observed between 40 km/h and 60 km/h for both the horizontal and vertical discrepancies ($p < 0.001$ in both cases), indicating that vehicle speed influences the magnitude of deviations in mesh capture. Similarly, the analysis of traffic lane direction showed significant differences between outbound and inbound trajectories for both discrepancies ($p = 0.0107$ for horizontal and $p < 0.001$ for vertical). These findings suggest that both speed and lane direction are critical factors affecting the distribution of discrepancies, highlighting the need to consider these variables in evaluating data accuracy.

While paired-sample *t*-tests have identified significant differences between specific speed and direction of travel conditions, these comparisons are limited by considering only pairs of groups. Applying the ANOVA to obtain a more comprehensive and robust view of the behaviour of the variables analyzed is appropriate. First, the NET-factor ANOVA will allow the overall effect of speed and direction of travel to be evaluated separately, considering simultaneously all levels of each factor. Subsequently, the two-factor ANOVA will make it possible not only to contrast the main effects of speed and direction of travel, but also to determine the existence of potential interactions between the two, i.e., whether the influence of speed varies as a function of the direction of travel. This ensures a more complete and conclusive statistical analysis of the impact of the factors on discrepancies and Horizontal discrepancy.

A NET-factor ANOVA was conducted to assess the individual effects of speed and trajectory direction during data acquisition. Furthermore, a two-factor ANOVA was per-

formed to examine the combined influence of these factors on horizontal and vertical discrepancies. The results obtained are summarized in Tables 16–18, which present the summaries of the different ANOVA models applied.

Table 16. NET-factor ANOVA results for coordinate discrepancies across speed.

Variable	Source of Variation	Df	Sum Sq (m^2)	Mean Sq (m^2)	F Value	*p*-Value	Signif.
Horizontal Discrepancy	Factor (Speed)	1	0.0228	0.0228	16.11	0.00009	***
	Error	150	0.2123	0.00142			
	Total	151	0.2351				
Vertical Discrepancy	Factor (Speed)	1	0.00166	0.00166	3.682	0.0569	•
	Error	150	0.06782	0.00045			
	Total	151	0.06948				

Note: The significance codes indicate the level of statistical significance associated with the *p*-values as follows: *** for $p < 0.001$, ** for $p < 0.01$, * for $p < 0.05$, • for $p < 0.1$, and a blank space for $p \geq 0.1$, indicating no statistical significance.

Table 17. NET-factor ANOVA results for horizontal and vertical discrepancies across trajectory direction (TD).

Variable	Source of Variation	Df	Sum Sq (m^2)	Mean Sq (m^2)	F Value	*p*-Value	Signif.
Horizontal Discrepancy	Factor (Lane)	1	0.00261	0.00261	1.683	0.197	
	Error	150	0.23252	0.00155			
	Total	151	0.23513				
Vertical Discrepancy	Factor (Lane)	1	0.00078	0.00078	1.71	0.193	
	Error	150	0.0687	0.00046			
	Total	151	0.06948				

Note: The significance codes indicate the level of statistical significance associated with the *p*-values as follows: *** for $p < 0.001$, ** for $p < 0.01$, * for $p < 0.05$, • for $p < 0.1$, and a blank space for $p \geq 0.1$, indicating no statistical significance.

Table 18. Two-factor ANOVA results for coordinate discrepancies (across speed and TD).

Variable	Source of Variation	Df	Sum Sq (m^2)	Mean Sq (m^2)	F Value	*p*-Value	Signif.
Horizontal Discrepancy	Factor (Speed)	1	0.0228	0.0228	16.238	0.000089	***
	Factor (Lane)	1	0.00261	0.00261	1.858	0.175	
	Factor (Speed × Lane)	1	0.00191	0.00191	1.357	0.246	
	Error	148	0.20782	0.0014			
	Total	151	0.23514				
Vertical Discrepancy	Factor (Speed)	1	0.00166	0.00166	3.721	0.0556	•
	Factor (Lane)	1	0.00078	0.00078	1.751	0.1878	
	Factor (Speed × Lane)	1	0.00083	0.00083	1.853	0.1754	
	Error	148	0.0662	0.00045			
	Total	151	0.06947				

Note: The significance codes indicate the level of statistical significance associated with the *p*-values as follows: *** for $p < 0.001$, ** for $p < 0.01$, * for $p < 0.05$, • for $p < 0.1$, and a blank space for $p \geq 0.1$, indicating no statistical significance.

The results of the ANOVA (Tables 16–18) allow a comprehensive evaluation of the influence of speed and traffic lane on the discrepancies analyzed. The one-factor ANOVA considering speed (Table 16) showed a statistically significant effect of this variable on the horizontal discrepancy ($F = 16.11$; $p < 0.001$), confirming that higher speeds are associated with higher deviations in planimetric accuracy. In contrast, the vertical discrepancy did not reach conventional levels of significance ($F = 3.68$; $p = 0.057$), although the value close to the threshold suggests a possible trend that deserves consideration.

When trajectory direction was analyzed as the only factor (Table 17), no significant differences were observed for either horizontal or vertical discrepancies ($p > 0.1$ in both cases). This indicates that the direction of movement at the time of data capture by itself does not exert a relevant influence on the accuracy of the point grids.

The two-factor ANOVA (Table 18) confirmed the predominant role of speed as the main explanatory factor for horizontal discrepancy (F = 16.24; $p < 0.001$), while neither the direction of information capture nor the interaction between speed and capture direction were statistically significant. In the case of vertical discrepancy, none of the factors or their interaction reached significance, although speed again showed a marginal trend (F = 3.72; $p = 0.056$).

These results show that vehicle speed is the critical factor affecting horizontal accuracy, while the traffic lane has no appreciable effect. Vertical discrepancies, on the other hand, are less sensitive to both speed and lane, although they show a slight tendency to increase with higher speeds. The absence of interaction effects suggests that the influence of speed on accuracy remains constant regardless of the lane travelled.

Figure 8 presents boxplots of the horizontal and vertical discrepancies as a function of vehicle speed (40 and 60 km/h) and traffic lane (Outbound and Inbound). These graphical representations complement the results of the analysis of variance, allowing a direct visual inspection of the distribution of the data, the variability observed in each condition, and the possible existence of differences between groups. The figures include the main descriptive statistics (minimum, quartiles, median, and maximum), providing a more intuitive view of the experimental factors' influence on the measurements' precision.

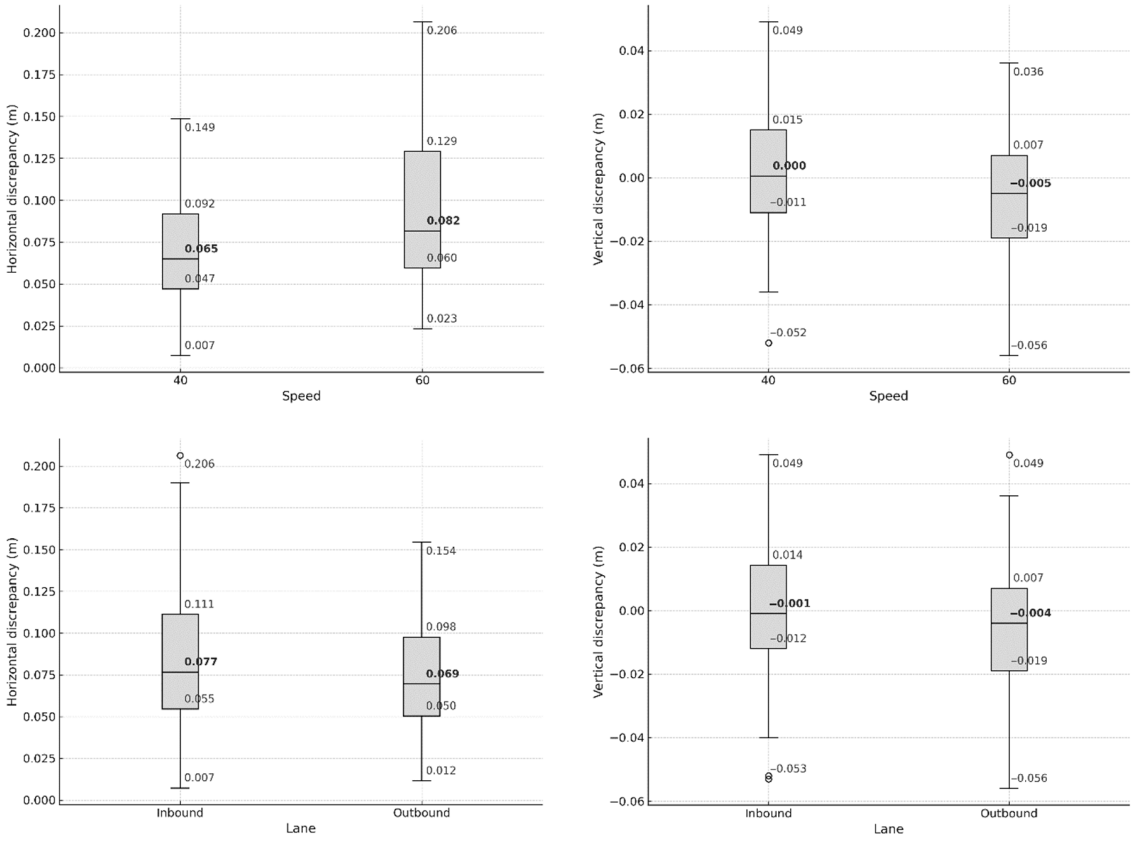


Figure 8. Distribution of horizontal and vertical discrepancies is represented by boxplots, according to vehicle speed (40 and 60 km/h) and traffic lane (Outbound and Inbound). The bold values denote the statistical median.

The box plots confirm the statistical findings of the ANOVA. Regarding speed, there is a clear increase in horizontal discrepancy at 60 km/h compared to 40 km/h, with greater

dispersion and higher median values, supporting the significant effect detected in Table 15 ($p < 0.001$). Although small in magnitude, vertical discrepancies show slightly greater variability at higher speeds, in line with the marginal effect suggested by the ANOVA ($p \approx 0.056$). At the lane level, the distributions of horizontal and vertical discrepancies overlap widely, with very similar medians and interquartile ranges between Outbound and Inbound trajectories. This graphical evidence reinforces the absence of significant differences reported in Table 16. Overall, the figures visually illustrate that speed is the main factor affecting horizontal accuracy, while traffic lane has no appreciable influence, and vertical discrepancies remain relatively stable in all conditions.

In addition to the ANOVA, the RMSE was calculated as an integrated indicator of positional accuracy (Table 19). Unlike the ANOVA, which assesses the statistical significance of differences between groups, the RMSE provides a synthetic measure that simultaneously accounts for horizontal and vertical discrepancies, thereby offering a global perspective of system performance. The results confirm the findings of the ANOVA, highlighting the degradation of accuracy at higher speeds and the greater influence of trajectory direction on the vertical component. Furthermore, the RMSE facilitates direct comparison of overall errors across experimental conditions, making it a useful and widely accepted indicator in geospatial accuracy assessment. Its inclusion, therefore, strengthens the analysis by combining statistical rigour with a practical measure of error magnitude that is more directly interpretable for engineering applications.

Table 19. RMSE values for speed, trajectory direction, and interactions.

Factor		Horizontal Discrepancy (m)	Vertical Discrepancy (m)	RMSE (Z + Horizontal) (m)
Speed (km/h)	40	0.021	0.075	0.055
	60	0.022	0.101	0.073
Trajectory direction	Outbound	0.022	0.083	0.061
	Inbound	0.021	0.094	0.068
Interactions	40-Outbound	0.021	0.073	0.054
	40-Inbound	0.021	0.076	0.056
	60-Outbound	0.024	0.092	0.067
	60-Inbound	0.020	0.109	0.078

The analysis of the RMSE values presented in Table 19 highlights the relative influence of speed and trajectory direction on positional accuracy. Regarding speed, results indicate a clear degradation of accuracy at higher velocities. At 60 km/h, both horizontal discrepancy (0.022) and planimetric error (0.101) increase compared to 40 km/h (0.021 and 0.075, respectively), which results in a higher overall RMSE (0.073 vs. 0.055). These findings confirm that increased acquisition speed negatively affects data precision, particularly in the horizontal dimension.

Although RMSE values did not differ significantly between 40 km/h and 60 km/h in the analyzed segment, previous MMS studies have shown that vehicle speed can influence the behaviour and orientation of scan profiles, potentially introducing small trajectory instabilities that may accumulate over longer linear surveys [32,33]. Such effects may not be reflected in pointwise RMSE over short stretches but can affect the geometric consistency of longer acquisitions. This consideration is conceptual and does not contradict the empirical results obtained in this study.

Regarding the direction of travel, the results show a more moderate but still evident effect. Inbound trajectories yield higher discrepancies in the vertical component (0.094 vs. 0.083 for Outbound) and a larger global RMSE (0.068 vs. 0.061), whereas horizontal discrepancies remain nearly constant between directions. This suggests that the

main contribution of trajectory direction to reduced accuracy arises from its influence on the vertical component rather than on horizontal coordinates.

Finally, the analysis of the interactions between speed and trajectory direction reinforces these observations. The lowest RMSE values are found at 40 km/h, particularly in the Outbound condition (0.054), whereas the highest values occur at 60 km/h in the Inbound direction (0.078). This pattern demonstrates that, although trajectory direction modulates accuracy somewhat, the dominant factor is travel speed, whose effect is consistently reflected in higher RMSE values across conditions.

4. Discussion

The relevance of evaluating MMS performance under real operating conditions is supported by recent reviews, which emphasize that trajectory accuracy is one of the main limiting factors in the geometric quality of mobile mapping data. Errors in GNSS/INS integration propagate directly into the georeferenced point cloud, particularly affecting vertical consistency and the alignment between overlapping strips [34]. This highlights the importance of examining how differential correction strategies and acquisition speed influence the final 3D accuracy, as these parameters directly shape the stability and reliability of the estimated trajectory.

The results show that the three differential correction strategies evaluated (NET, VRS, and MBS) present an equivalent behaviour in the horizontal plane, which indicates that, from a planimetric perspective, any of them can guarantee an adequate level of accuracy for road mapping applications. The accuracy of LiDAR systems in horizontal measurements, which are subject to possible noise due to reflection on the road surface, matches this magnitude and compares with the greater accuracy of measurements taken in the altimetric component. Furthermore, identifying significant points in the point cloud on the road markings, such as corners of broken lines and their resolution (4–6 cm depending on the speed of the MMS), means that horizontal accuracy is limited to these values.

However, the analysis of the vertical component reveals significant differences that should not be overlooked. The NET strategy, based on a nearby physical station, is more consistent and with less dispersion in the Z component, while VRS and MBS register larger discrepancies. This behaviour may be related to how the corrections are generated and transmitted: in NET, the reference comes from a fixed and stable station, while in VRS and MBS, there are factors associated with the spatial interpolation of the network or the temporal installation of the base station that intervene. This finding suggests that altimetric accuracy depends more strongly on the robustness and stability of the correction strategy, which should be considered especially in projects requiring three-dimensional modelling or infrastructure assessment, where the vertical axis is critical.

The analysis of operational factors shows that the speed at which the vehicle travels is the most critical determinant of data quality. The increase in horizontal and, to a lesser extent, vertical discrepancy from 40 to 60 km/h highlights the loss of geometric stability and point density implied by a higher acquisition rate. Although the numerical differences may seem small, this effect translates into a cumulative impact when dealing with extensive coverage, compromising the homogeneity and reliability of the survey. In contrast, the traffic lane has a much more limited influence: the horizontal discrepancies remain practically constant between Outbound and Inbound, while the vertical component shows slight variations that probably respond more to the geometry of the road (camber, slopes, proximity of embankments or ditches) than to the fact of driving in one lane or the other. In this sense, the direction of travel does not appear to be a structural factor, although it can act as a modulator under certain topographical or environmental conditions.

The joint consideration of correction strategies and operational factors reveals a clear pattern: while the horizontal discrepancy remains stable and relatively robust to changes in configuration, the vertical discrepancy is more sensitive to both the strategy used and the travel speed. This implies that altimetric errors are the most critical component in mobile capture, and that their mitigation requires a two-pronged approach: carefully choosing the most appropriate differential correction strategy for the context and strictly controlling the acquisition operating conditions. This conclusion is particularly relevant when 3D models derived from MMS are used for advanced planning tasks, simulation in virtual environments, or support for autonomous driving, where even minor vertical deviations can have significant consequences.

5. Conclusions

The results show that the quality of the data generated by a mobile mapping system does not depend exclusively on the instrumentation used, but rather on the interaction between differential correction strategies and operational acquisition conditions. Although horizontal discrepancies remain stable and resistant to methodological and operational changes, the vertical component is more vulnerable, making it the critical factor in ensuring the overall reliability of the derived products.

This behaviour highlights the importance of carefully selecting the differential correction strategy and maintaining operating conditions that bring geometric stability, especially regarding vehicle travel speed. Tests show that slight variations in these variables can translate into noticeable differences in the final quality of three-dimensional models, which have direct implications for high-demand applications such as infrastructure planning, advanced simulation, or autonomous mobility support. It has also been demonstrated that LiDAR measurements in MMS allow for high relative accuracy (within the scan profile) and that lower overall absolute accuracy allows for better adjustment of direct measurements made with a GNSS reference base located in the vicinity of the road at less than 5 km, as demonstrated by the MBS solution.

The results of the analyses of the influence of acquisition speed and the type of differential correction can form the basis for establishing a reference framework on which to select the operating parameters for road surveys using MMS. Using moderate acquisition speeds and robust GNSS differential correction methods allows for consistent mapping in terms of geometric accuracy.

However, the scope of this research is limited to a rural two-lane environment under relatively controlled environmental conditions. The results may vary in other contexts, where factors related to GNSS data capture, such as signal obstruction or multipath effects, may introduce additional errors. Therefore, it could be interesting to extend the study to more complex scenarios to validate the robustness of the results in situations other than those considered.

Finally, beyond purely geometric considerations, addressing the operational efficiency of surveys carried out using MMS is essential. In addition to metric accuracy, it is necessary to consider the resources required for data acquisition, particularly in terms of time and processing. In this context, the vehicle speed is a determining parameter, as it directly influences the density of points captured and the amount of information that must be managed. It is essential to maintain adequate speeds to ensure geometric stability. This is achieved by minimizing vibrations, misalignments, and synchronization delays of GNSS/INS and photographic sensors, as well as LiDAR systems. The results indicate that an acquisition speed of 40 km/h is a practical compromise between sampling density, geometric stability of the system, and operational productivity requirements, thus ensuring the metric quality of the models generated.

Overall, the results reinforce the idea that optimizing mobile mapping surveys requires an integrated approach that combines methodological and operational decisions. This approach minimizes the discrepancies observed and ensures that the data obtained effectively meets the accuracy and consistency requirements of the most advanced application environments.

The results obtained underscore the necessity of adopting more complete evaluation frameworks that concurrently assess GNSS corrective behaviour, sensor dynamic stability, and environmental geometric fluctuations. The integration of assessments across these dimensions will provide a more precise characterization of the MMS's overall response to various configurations and operating situations. This will aid in creating more rigorous criteria for organizing mobile surveys and will encourage the establishment of standardized procedures that ensure the consistency and dependability of three-dimensional goods produced in road engineering and infrastructure applications.

Author Contributions: Conceptualization, L.I. and S.L.-C.; methodology, L.I. and S.L.-C.; validation, L.I.; formal analysis, L.I., S.L.-C., R.R.-S. and M.C.; investigation, L.I., S.L.-C., R.R.-S. and M.C.; data curation, S.L.-C., and R.R.-S.; writing—original draft preparation, L.I., S.L.-C., R.R.-S. and M.C.; writing—review and editing, L.I. and M.C.; supervision, M.C.; project administration, M.C.; funding acquisition, L.I. and M.C. All authors have read and agreed to the published version of the manuscript.

Funding: Grant PID2021-122471OB-I00 funded by MICIU/AEI/10.13039/501100011033 and by ERDF/EU.

Data Availability Statement: The original data presented in the study are openly available in e-cienciaDatos at https://doi.org/10.21950/9KSH9C, accessed on 11 November 2025.

Conflicts of Interest: The authors declare no conflicts of interest.

Abbreviations

The following abbreviations are used in this manuscript:

AADT	Annual Average Daily Traffic
CC-BY 4.0	License Creative Commons Atribución 4.0 Internacional
CI	Confidence Interval
CNIG	National Centre for Geographic Information of Spain
ERMS	Ellipsoidal Root Mean Square
GLONASS	Global Navigation Satellite System
GPS	Global Positioning System
HRMS	Horizontal Root Mean Square
HSD	Honestly Significant Difference
IGN	National Geographic Institute of Spain
IMU	Inertial measurement units
INS	Inertial navigation system
LiDAR	Light Detection and Ranging
MBS	Mobile Base Station
MMS	Mobile Mapping System
NET	Network GNSS solution of the National Geographic Institute for differential correction
NRMS	Normalized Root Mean Square
PNOA	National Aerial Orthophotography Plan of Spain
PS-InSAR	Interferometric Synthetic Aperture Radar
RMSE	Root mean square error
RTK	Real-Time Kinematic

SBAS	Satellite-Based Augmentation System
SfM	Structure from Motion
TERRASTAR	TerraStar Correction Service
UAV	Unmanned Aerial Vehicle
VRMS	Vertical Root Mean Square
VRS	Virtual reference stations for differential correction
ZUP	Zero velocity UPdaTe

References

1. Khoramshahi, E.; Nezami, S.; Pellikka, P.; Honkavaara, E.; Chen, Y.; Habib, A. A taxonomy of sensors, calibration and computational methods, and applications of mobile mapping systems: A comprehensive review. *Remote Sens.* **2025**, *17*, 1502. [CrossRef]
2. Ali, A.; Aziz, M.; Rasool, A.M.; Ali, U.; Umar, M.; Wani, K.M.N.S. Applications of remote sensing technologies to assess ground displacements and seismic hazards: Precision, scale, and insight. *Arab. J. Sci. Eng.* **2025**, *50*, 16357–16378. [CrossRef]
3. Oh, J.; Shin, S.; Lee, C.; Lee, J. Establishment of point cloud location accuracy evaluation facility for car-mounted mobile mapping system. *J. Korean Soc. Surv. Geod. Photogramm. Cartogr.* **2020**, *38*, 383–390. [CrossRef]
4. Hwang, J.; Shin, S.; Lee, J.; Lee, J. Positioning accuracy enhancement of land-based mobile mapping system for updating national base map. *J. Cadastre Land Inf. (JCLI)* **2011**, *41*, 201–214.
5. Toschi, I.; Nocerino, E.; Menna, F.; Remondino, F.; Rodolà, E. Accuracy evaluation of a mobile mapping system with advanced statistical methods. *Int. Arch. Photogramm. Remote Sens. Spat. Inf. Sci.* **2015**, *XL-5/W4*, 245–252. [CrossRef]
6. Toth, C.; Grejner-Brzezinska, D. Redefining the paradigm of modern mobile mapping: An automated high-precision road centerline mapping system. *Photogramm. Eng. Remote Sens.* **2004**, *70*, 685–694. [CrossRef]
7. Javanmardi, M.; Javanmardi, E.; Gu, Y.; Kamijo, S. Towards high-definition 3D urban mapping: Road feature-based registration of mobile mapping systems and aerial imagery. *Remote Sens.* **2017**, *9*, 975. [CrossRef]
8. Viler, F.; Cefalo, R.; Sluga, T.; Snider, P.; Pavlovčič-Prešeren, P. The efficiency of geodetic and low-cost GNSS devices in urban kinematic terrestrial positioning in terms of the trajectory generated by MMS. *Remote Sens.* **2023**, *15*, 957. [CrossRef]
9. Zhang, Z.; Li, Y.; He, X.; Hsu, L. Resilient GNSS real-time kinematic precise positioning with inequality and equality constraints. *GPS Solut.* **2023**, *27*, 116. [CrossRef]
10. Martínez-Sánchez, J.; Nogueira, M.; González-Jorge, H.; Solla, M.; Arias, P. SITEGI project: Applying geotechnologies to road inspection. Sensor integration and software processing. *ISPRS Ann. Photogramm. Remote Sens. Spat. Inf. Sci.* **2013**, *II-5/W2*, 181–186. [CrossRef]
11. Khoramshahi, E.; Campos, M.B.; Tommaselli, A.M.G.; Vilijanen, N.; Mielonen, T.; Kaartinen, H.; Kukko, A.; Honkavaara, E. Accurate calibration scheme for a multi-camera mobile mapping system. *Remote Sens.* **2019**, *11*, 2778. [CrossRef]
12. Kersting, A.P.; Habib, A.; Rau, J. New method for the calibration of multi-camera mobile mapping systems. *Int. Arch. Photogramm. Remote Sens. Spat. Inf. Sci.* **2012**, *39*, 121–126. [CrossRef]
13. Chan, T.O.; Lichti, D.D.; Glennie, C.L. Multi-feature based boresight self-calibration of a terrestrial mobile mapping system. *ISPRS J. Photogramm. Remote Sens.* **2013**, *82*, 112–124. [CrossRef]
14. Hillemann, M.; Weinmann, M.; Mueller, M.S.; Jutzi, B. Automatic extrinsic self-calibration of mobile mapping systems based on geometric 3D features. *Remote Sens.* **2019**, *11*, 1955. [CrossRef]
15. Ravi, R.; Lin, Y.-J.; Elbahnasawy, M.; Shamseldin, T.; Habib, A. Simultaneous system calibration of a multi-LiDAR multicamera mobile mapping platform. *IEEE J. Sel. Top. Appl. Earth Obs. Remote Sens.* **2018**, *11*, 1694–1714. [CrossRef]
16. Bao, S.; Shi, W.; Chen, P.; Xiang, H. Sole GNSS sensor extrinsic calibration methods for mobile mapping systems. *IEEE Robot. Autom. Lett.* **2022**, *7*, 11338–11345. [CrossRef]
17. Ravi, R.; Habib, A. Fully automated profile-based calibration strategy for airborne and terrestrial mobile LiDAR systems with spinning multi-beam laser units. *Remote Sens.* **2020**, *12*, 401. [CrossRef]
18. Hong, S.; Park, I.; Lee, J.; Lim, K.; Choi, Y.; Sohn, H.-G. Utilization of a terrestrial laser scanner for the calibration of mobile mapping systems. *Sensors* **2017**, *17*, 474. [CrossRef]
19. Brogan, M.; McLoughlin, S.; Deegan, C. Assessment of stereo camera calibration techniques for a portable mobile mapping system. *IET Comput. Vis.* **2013**, *7*, 209–217. [CrossRef]
20. Soilán, M.; González-Aguilera, D.; del-Campo-Sánchez, A.; Hernández-López, D.; Del Pozo, S. Road marking degradation analysis using 3D point cloud data acquired with a low-cost Mobile Mapping System. *Autom. Constr.* **2022**, *141*, 104446. [CrossRef]
21. Mizutani, T.; Yamaguchi, T.; Kudo, T.; Yamamoto, K.; Ishida, T.; Nagata, Y.; Kawamura, H.; Tokuno, T.; Suzuki, K.; Yamaguchi, Y. Quantitative evaluation of peeling and delamination on infrastructure surfaces by laser signal and image processing of 3D point cloud data. *Autom. Constr.* **2022**, *133*, 104023. [CrossRef]

22. Lehtomäki, M.; Kukko, A.; Matikainen, L.; Hyyppä, J.; Kaartinen, H.; Jaakkola, A. Power line mapping technique using all-terrain mobile laser scanning. *Autom. Constr.* **2019**, *105*, 102802. [CrossRef]
23. Domínguez, H.; Morcillo, A.; Soilán, M.; González-Aguilera, D. Automatic Recognition and Geolocation of Vertical Traffic Signs Based on Artificial Intelligence Using a Low-Cost Mapping Mobile System. *Infrastructures* **2022**, *7*, 133. [CrossRef]
24. Community of Madrid, Directorate-General for Traffic. Traffic-IMD. 2023. Available online: https://www.comunidad.madrid/servicios/transporte/estudio-intensidad-media-diaria-vehiculos-imd (accessed on 2 October 2025).
25. National Centre for Geographic Information (CNIG). *Physical Map*. National Geographic Institute. 2022. Available online: https://centrodedescargas.cnig.es (accessed on 1 December 2025).
26. Zoller+Fröhlich GmbH. (n.d.) Z+F PROFILER® 9020|9020-2, 2D Laser Scanner. Z+F (Zofre). Available online: https://www.zofre.de/en/laser-scanners/2d-laser-scanner/z-f-profiler-9020 (accessed on 21 August 2025).
27. GIM International. Pathway Services Selects iXBlue's New ATLANS C. 2014. Available online: https://www.gim-international.com/content/news/pathway-services-selects-ixblue-s-new-atlans-c?output=pdf (accessed on 21 August 2025).
28. Zoller+Fröhlich GmbH. (n.d.) Z+F MapCam® C, Laserscanning Accessory. Available online: https://www.zofre.de/en/laser-scanners/laser-scanner-accessories/z-f-mapcamr-c (accessed on 21 August 2025).
29. Urquizo Ingenieros. Urquizo Ingenieros | Topografía en Bilbao (Bizkaia). 2025. Available online: https://urquizoingenieros.xyz/ (accessed on 1 December 2025).
30. Janssen, V. A comparison of the VRS and MAC principles for network RTK. In Proceedings of the IGNSS Symposium 2009, Surfers Paradise, Australia, 1–13 December 2009; Available online: https://hdl.handle.net/102.100.100/493475 (accessed on 1 December 2025).
31. GeoMax/eGPS Solutions. GeoMax Zenith40 GNSS Receiver Datasheet. 2019. Available online: https://www.egps.net/datasheets/GeoMax-Zenith40-GNSS-Receiver-Datasheet.pdf (accessed on 9 October 2025).
32. Cahalane, C.; McElhinney, C.P.; McCarthy, T. Mobile mapping system performance: An analysis of the effect of laser scanner configuration and vehicle velocity on scan profiles. In *European Laser Mapping Forum (ELMF 2010)*; National University of Ireland Maynooth: Maynooth, Ireland, 2010.
33. Shi, B.; Bai, Y.; Zhang, S.; Zhong, R.; Yang, F.; Song, S.; Li, G. Reference-plane-based approach for accuracy assessment of mobile mapping point clouds. *Measurement* **2021**, *171*, 108759. [CrossRef]
34. Pöppl, F.; Neuner, H.; Mandlburger, G.; Pfeifer, N. Integrated trajectory estimation for 3D kinematic mapping with GNSS, INS and imaging sensors: A framework and review. *ISPRS J. Photogramm. Remote Sens.* **2023**, *196*, 287–305. [CrossRef]

Disclaimer/Publisher's Note: The statements, opinions and data contained in all publications are solely those of the individual author(s) and contributor(s) and not of MDPI and/or the editor(s). MDPI and/or the editor(s) disclaim responsibility for any injury to people or property resulting from any ideas, methods, instructions or products referred to in the content.